The composition and weathering of the continents over geologic time

A.G. Lipp, O. Shorttle, E.A. Sperling, J.J. Brocks, D. Cole, P.W. Crockford, L. Del Mouro, K. Dewing, S.Q. Dornbos, J.F. Emmings, U.C. Farrell, A. Jarrett, B.W. Johnson, P. Kabanov, C.B. Keller, M. Kunzmann, A.J. Miller, N.T. Mills, B. O'Connell, S.E. Peters, N.J. Planavsky, S.R. Ritzer, S.D. Schoepfer, P.R. Wilby, J. Yang

Supplementary Information

The Supplementary Information includes:

- Supplementary Information on Data and Methods
- Tables S-1 to S-3
- Figures S-1 to S-5
- Supplementary Information References

Supplementary Information on Data and Methods

An annotated R-markdown notebook which performs all the calculations described below in R and python can be found at github.com/AlexLipp/crustal-comp (Van Rossum and Drake, 2009; R Core Team, 2018). The data used for our reported results and the SQL command used to query the SGP database are also found at the same location. This repository is archived at the point of submission at doi.org/10.5281/zenodo.4309952.

Data

The Sedimentary Geochemistry and Paleoenvironments Project (SGP) is a research consortium that has produced the largest available compilation of sedimentary geochemical data from across Earth's history. This compilation is being analysed for a range of different research questions, in addition to this study. The project combines pre-existing large datasets, such as the United States Geological Survey (USGS) National Geochemical Database and Critical Metals in Black Shales compilations, with new data gathered from temporal gaps identified in the record. Each sample in the dataset is accompanied with contextual data relating to their stratigraphic and geographic position, including an interpreted absolute age. More information can be found at the project's homepage at sgp.stanford.edu/about. The

current phase of SGP focuses primarily on the Phanerozoic and so for the Precambrian aspects of this study it was supplemented with the compilation from Lipp *et al.* (2020) and further literature data (Fedo *et al.*, 1996; Nesbitt *et al.*, 2009; Devaraju *et al.*, 2010). A histogram of how these samples are distributed in time is given in Figure S-1.

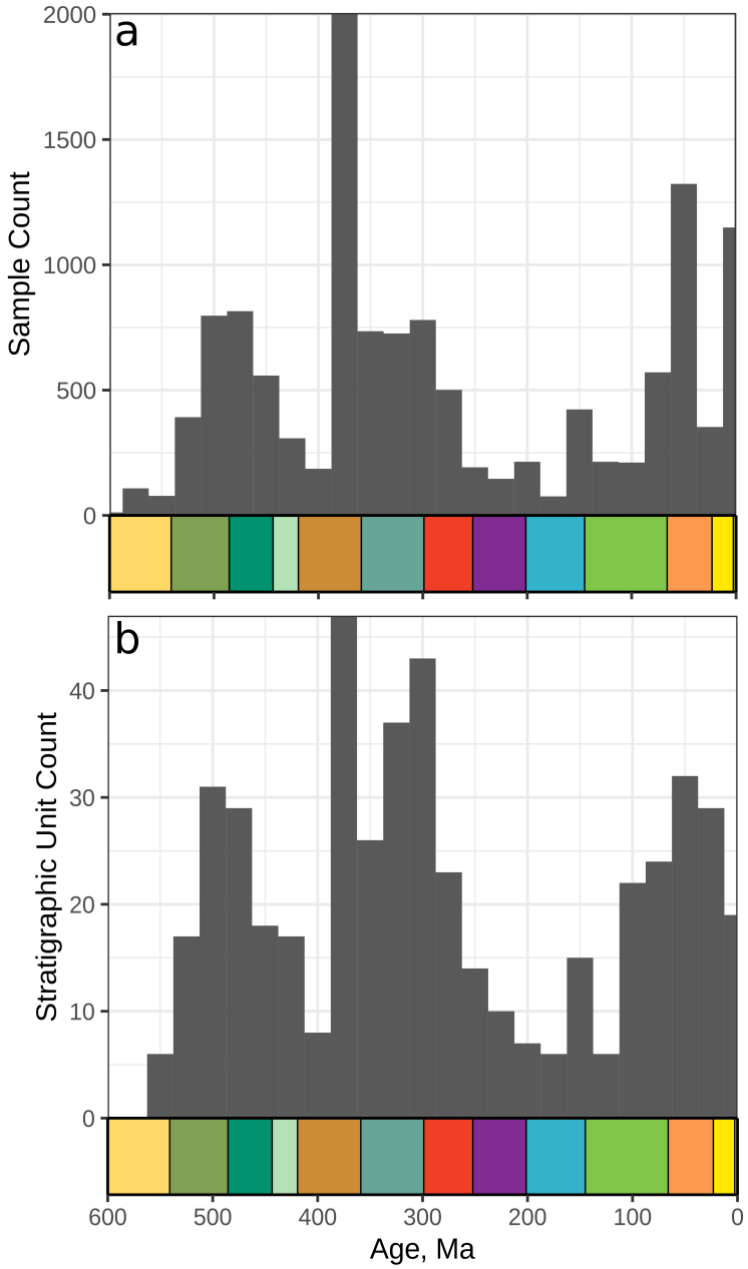

Figure S-1 Temporal sampling density of dataset. **(a)** Histogram of ages for all samples included in dataset with binwidth equal to 25 Myr. Coloured boxes indicate geological periods (see Fig. 3). **(b)** Same as panel (a) but for the number of individual stratigraphic units sampled, as defined by the SGP dataset.

From this database, we query for samples which contain measurements of all the seven elements required for our method (Si, Al, Mg, Fe, Na, Ca, K), by any analytical method except for Handheld X-Ray Fluorescence (HHXRF). HHXRF is excluded as it is sensitive to sample preparation which cannot easily be controlled for potentially introducing artefacts. Additionally, HHXRF cannot reliably produce data for Mg and Na, both of which are required for our data

analysis (Young *et al*., 2016). In any large data compilation, there are concerns about underlying data quality. Because our analyses require Si, and we have excluded HHXRF data, most data will have been generated using benchtop XRF instruments. The higher abundance of XRF data is because ICP methodologies frequently do not produce Si data, although this depends on the sample dissolution protocol used. As most data is generated by one methodology, possible biases between analyses are reduced. Additionally, individual measurement errors will not affect overall patterns in large datasets as long as there are not systematic biases in the dataset (*e.g*., Sepkoski, 1993). It is thus unlikely there are errors resulting from original analyses that are driving our results. Further, almost all data are from the published literature or accredited laboratories (*e.g*., USGS data) and therefore meet these levels of independent community approval. Thus, geochemical measurement errors are unlikely to affect our results.

The data presented here is compiled from hundreds of sources, mostly from the peer-reviewed academic literature. Whilst precautions have been applied to ensure a high-quality of data, and much of the data has already been scrutinised under peer-review, it is not possible to independently verify it in this study. The data presented should be treated with the same scrutiny applied to any published data.

After obtaining these data, the elemental compositions are converted into wt. % oxides, with total iron given as Fe_2O_3. The results of our method are the same whether or not the composition is normalised to 100 % prior to analysis.

Data Screening

To ensure the reliability of our input data, we screen certain samples from the data extracted from the SGP database. First, we remove any manually identified duplicates which are present due to overlap between the literature compilation of Lipp *et al*. (2020) and any literature data within the SGP dataset. Second, we exclude any samples for which the lithology is not listed as siliciclastic. Finally, from these siliciclastic sediments we exclude samples which are likely to have been affected by carbonate contamination. How these carbonate contaminated samples are identified is described in further detail below.

Composite Samples

Composite sediment samples are generated by mixing (*i.e*. taking the arithmetic mean) of all samples within 500 Ma intervals (Table S-1). Due to low sample density in the Archean, all samples older than 2.5 Ga were mixed to generate an Archean composite. If composite samples are created in 500 Ma bins in the Archean, there are some minor changes to the results. The 3.5–4.0 Ga interval produces an Andesitic protolith, and the 3.0–3.5 Ga has a protolith similar to that from the time period 0–0.5 Ga. However, given the low sampling density (the 3.5–4.0 Ga interval contains only 30 samples all from the Isua Greenstone Belt), this temporal variance is likely strongly affected by local variability. There is no reasonable binning procedure which results in a protolith of any time-interval more mafic than an Andesite.

Table S-1 Composite sediment compositions through time.

Age, Ga	SiO_2	Al_2O_3	$Fe_2O_3^T$	MgO	Na_2O	CaO	K_2O
0–0.5	71.7	13.7	5.12	2.35	1.14	2.99	3.06
0.5–1.0	70.0	15.6	5.42	2.18	1.26	1.79	3.77
1.0–1.5	68.4	16.4	5.97	2.34	1.32	1.53	4.08
1.5–2.0	66.6	17.1	6.00	2.51	1.09	2,13	4.58
2.0–2.5	66.0	17.6	7.46	2.41	1.86	1.25	3.46
2.5 +	65.1	17.0	7.70	3.29	2.08	1.84	3.00

Phanerozoic paleoclimate

The detrended Oxygen isotope composition of carbonates shown in Figure 3 of the main manuscript was generated by smoothing (with a 30 Myr bandwidth Gaussian data from $\delta^{18}O$ compilation of Jaffrés *et al*. (2007). Periods of glaciation (star emphasises the shortlived Gaskiers glaciation) are taken from Pu *et al*. (2016) and Macdonald *et al*. (2019). The period of land plant expansion is considered as the period of the growth of alluvial mudrock in McMahon and Davies (2018), a proxy for land-plant expansion.

Data Analytical Methods

The method we use was developed and detailed in full in Lipp *et al*. (2020). This method deconvolves the major-element composition of a sediment into the contribution due to changes in protolith and changes caused by chemical weathering. This method has a number of benefits relative to previous compositional analytical approaches such as: insensitivity to the issues of the 'closure effect', the ability to reconstruct the full composition of protoliths, and a quantitative measure of misfit.

This approach works by constructing a 2D vector addition model to explain the major-element compositions of sediments. This model is shown in Equation 1 in the main manuscript and repeated here:

$$\mathbf{x'} = \mathbf{UCC} + \omega\hat{\mathbf{w}} + \psi\hat{\mathbf{p}} + \mathbf{E}. \qquad \text{(Eq. 1)}$$

This model is only applied to a composition, **x**, after they have undergone a centred log-ratio, *clr*, transformation to resolve the 'closure' effect inherent to compositional data (Aitchison 1986). Hence, *clr*(**x**) = **x'**. The unit vectors corresponding to weathering and protolith, $\hat{\mathbf{w}}$ and $\hat{\mathbf{p}}$ respectively, were calibrated on independent data. $\hat{\mathbf{w}}$ was calibrated using a soil profile, and $\hat{\mathbf{p}}$ was calibrated using a suite of cogenetic igneous rocks. The model calibrated in this way was successful in extracting information of weathering intensity and protolith from sedimentary compositions and explained the majority of the observed variance. However, residual analysis indicated two potential points at which the model could be improved.

First, $\hat{\mathbf{w}}$ was noted to be slightly miscalibrated, causing a systematic increase in misfit with increasing weathering intensity. This miscalibration was likely caused by calibrating $\hat{\mathbf{w}}$ on a single profile, which will incorporate localised noise. For this study, to derive a better calibrated vector we take a 'consensus' $\hat{\mathbf{w}}$ of two different profiles. Specifically, it is the arithmetic mean of the first principal components of the soil profile reported in White *et al*. (2001) and the 'Toorongo' soil profile that was used individually to calibrate the original $\hat{\mathbf{w}}$. This better calibrated $\hat{\mathbf{w}}$ ameliorates the issue of rising misfit with greater weathering intensity. All the vectors utilised in Equation 1 are given in Table S-2.

Table S-2 Centred log-ratio transformed vectors used to solve Equation 1.

	SiO_2	Al_2O_3	$Fe2O3^T$	MgO	Na_2O	CaO	K_2O
UCC	2.33	0.869	-0.142	-0.957	-0.681	-0.587	-0.836
$\hat{\mathbf{w}}$	0.242	0.369	0.235	0.133	-0.487	-0.678	0.186
$\hat{\mathbf{p}}$	0.234	0.098	-0.231	-0.601	0.248	-0.336	0.589

Secondly, a relationship between *clr*(Ca) and *clr*(Na) residuals was noted. This relationship was interpreted to be related to cation exchange of Ca and Na which is increasingly recognised as playing a significant impact on geochemical cycles (Sayles and Mangelsdorf, 1979; Cerling *et al*., 1989; Lupker *et al*., 2016). Subsequently it was observed that

cation exchange could cause, minor, spurious changes in ω and ψ if it was not explicitly taken into account. As a result, in this study we include a cation exchange correction into our model. Hence, our model is now:

$$\mathbf{x}' = \mathbf{UCC} + \omega\hat{\mathbf{w}} + \psi\hat{\mathbf{p}} + f(\chi) + \mathbf{E}.$$

This correction factor simply shifts compositions which have been offset from model plane due to cation exchange, back onto the 2D plane indicated in Equation 1. In this formulation $f(\chi)$ varies the proportion of total Ca and Na which taken up by Ca, χ, according to the stoichiometry:

$$Na_{2,clay} + Ca^{2+} \Leftrightarrow 2Na + Ca_{clay}.$$

χ therefore ranges between 0 and 1. $f(\chi)$ is nonlinear, so this equation has no analytical solutions. To find ω, ψ and χ we therefore numerically minimise $|\mathbf{E}|$ using a gradient descent algorithm implemented in python.

When increasing the components of any model there is always a trade-off between over and under-fitting data. We choose to explicitly consider cation exchange as a process as not doing so introduced some minor biases into our results. Nonetheless, this increases the risk that other processes not explicitly included in the model act to alias the results. We found that the major results of this study were invariant to including cation exchange or not.

Calculating Protolith Compositions

Consider a *clr* transformed major-element composition **x'**. We solve Equation 1 to calculate its ω and ψ values. These coefficients can be interpreted in terms of translating a protolith composition parallel to the weathering vector a distance equal to 'ω'. This translation is performed relative to a protolith composition equal to $\mathbf{UCC} + \psi\hat{\mathbf{p}}$. Hence, to calculate the protolith composition we simply translate back along the weathering vector to the original ω value. As a result, we need to calculate an ω value which corresponds to pristine igneous rocks, *i.e.* ω_0. Previously this was done by calculating the mean ω value of a large suite of igneous rocks taken from the NAVDAT (www.navdat.org) database (see Lipp *et al.*, 2020). Performing this calculation on the same compilation of igneous rocks for our updated $\hat{\mathbf{w}}$ vector gives an $\omega_0 = -0.271$.

Quantifying Uncertainties

Projecting all igneous variability onto a single 1D vector, $\hat{\mathbf{p}}$, is obviously a simplification, albeit a useful one. When we calculate protolith compositions as described above, any variability excluded from this 1D vector is neglected. A useful measure of uncertainity in the protolith calculations therefore is how much natural variability there is of real igneous rocks relative to this $\hat{\mathbf{p}}$ trend. To calculate this variability, we solve Equation 1 for the NAVDAT compilation of igneous rocks described above. The variability of igneous rocks around the trend, is hence the misfit matrix **E** for the NAVDAT dataset. If a multivariate gaussian uncertainity distribution is assumed we can therefore define $cov(\mathbf{E}_{NAVDAT})$. This covariance matrix is the closest multivariate analogy to a standard deviation for our estimates of protolith composition. $cov(\mathbf{E}_{NAVDAT})$ is given in Table S-3. To generate the uncertainty distributions shown in Figure 1 we simply add this derived $\mathbf{E}_{NAVDAT}$ matrix to the calculated *clr* protolith compositions, and then perform the inverse *clr* transformation. To turn this empirical distribution on the TAS plot into a confidence ellipse on Figure 1 we fit a 2D t-student distribution and demarcate the standard error of the mean ellipse, *i.e.* the 68.3 % interval.

Table S-3 Covariance matrix for reconstructed protoliths shown in Table 1. Note that this is for *clr* variables. This matrix is the closest multivariate analogy to a standard deviation.

	$c(SiO_2)$	$c(Al_2O_3)$	$c(Fe_2O_3)$	$c(MgO)$	$c(Na_2O)$	$c(CaO)$	$c(K_2O)$
$c(SiO_2)$	0.071	0.047	-0.050	-0.014	0.008	0.006	-0.068
$c(Al_2O_3)$	0.047	0.066	-0.039	-0.025	0.010	0.008	-0.068

c(Fe_2O_3)	-0.050	-0.039	0.132	-0.058	0.000	0.000	0.016
c(MgO)	-0.014	-0.025	-0.058	-0.062	-0.008	-0.007	0.050
c(Na_2O)	0.008	0.010	0.000	-0.008	0.003	0.001	-0.014
c(CaO)	0.006	0.008	0.000	-0.007	0.001	0.002	-0.010
c(K_2O)	-0.068	-0.068	0.016	0.050	-0.014	-0.010	0.094

Quantifying CO_2 drawdown

If a sediment's protolith composition is known, the relative loss of a specific element due to weathering can be calculated using the chemical depletion fraction, assuming an immobile element (*e.g.*, Brimhall and Dietrich, 1987; Jiang and Lee, 2019). In this study we calculate the sediment protolith composition, $\mathbf{x_0}$, from an observed composition, $\mathbf{x_1}$, using the method described above and use aluminium as an immobile element. Hence

$$f_i = \frac{\Delta M_i}{M_{i,0}} = \frac{x_{i,1}}{x_{i,0}} \cdot \frac{x_{\mathrm{Al_2O_3},0}}{x_{\mathrm{Al_2O_3},1}} - 1.$$

In this formulation, **f** is the kg of each component lost due to weathering for each kg of initial protolith, $M_{i,0}$ is the initial mass of the i^{th} component of a composition and ΔM_i is the change in mass of that same component due to weathering. Using this formula and Equation 1 it is possible to calculate the relative loss of each element due to weathering for a given ω–ψ pair. Converting from the mass of CaO and MgO lost to moles it is therefore possible to describe the ω–ψ plane in terms of maximum kg of CO_2 sequestered per kg protolith eroded (Fig. S-3a). This calculation assumes all weathering acidity is donated by carbonic acid and is therefore an upper-bound (Torres *et al.*, 2014). We note that the period 0–0.5 Ga has a lower ω than other periods, likely reflecting an increase in biogenic carbonate contamination bias relative to other time periods (see 'Carbonate addition bias' section below).

Potential biases and limitations

Diagenetic Alteration

There is increasing evidence that diagenetic reactions between terrestrial sediments and porefluids are significant parts of the geochemical cycle of many elements (Sun *et al.*, 2016). As the pH and geochemistry of porefluids evolves with depth, some primary minerals are dissolved, and reprecipitated as authigenic phases, changing the mineralogical composition of sediments as they are lithified. Three lines of evidence suggest our results have not been affected by this process. First, whilst these reactions affect mineralogy, so long as the reactions operate under closed-system conditions, use of bulk major-element data in aggregate is expected to be largely unaffected by this process. Given that the majority of siliciclastic sediments utilised in the SGP database are fine-grained and therefore low porosity, on this basis, closed system diagenesis is expected (Bjørlykke and Jahren, 2012). Assuming dominantly closed system diagenesis, our results should therefore be insensitive to diagenetic reactions. There is further evidence to support this assertion. Second, we can test the influence of diagenesis on the major element record of marine fine-grained sediments by comparing recent sedimentary rocks (0–0.5 Ga) to the major-element composition of the modern UCC as determined by surface sampling. This comparison shows that fine grained sediments produce a good match to the independently determined UCC composition. This suggests that diagenetic reactions have not biased the compositions of these recent sedimentary rocks. Finally, all of our principal findings are derived from aggregates of sediment geochemistry, either by generating composite samples (Table S-3), or by calculated a smoothed trend of noisy data (Fig. 3 in the main rticle). Hence, any diagenetic transfer of material within the sedimentary column will likely be undone to some degree during our data analytical process.

We emphasise here that our model is unable to indicate where or when a particular compositional process may have acted. For example, open system chemical weathering which acts in the subsurface (*e.g.*, anoxic marine silicate weathering; Wallmann *et al.*, 2008) could have the same compositional effect as chemical weathering which acts in a sediment source region. By extension, recycling of ancient sedimentary rocks could also impart an inherited weathering

signal into any subsequent sediments. The lack of a secular increase in weathering intensity over Earth's history suggests that this inheritance effect is not significant however.

Similarly, we have only explicitly considered cation exchange as acting on cations absorbed to clay particles. However, any reaction, diagenetic or otherwise, which is a net charge-balanced exchange of Ca for Na would produce the same compositional trend. This ambiguity is a limitation of any approach using purely elemental data.

Carbonate addition bias

Our model only explicitly considers the siliciclastic portion of a sediment. However, many sediments contain some portion of authigenic or biogenic carbonates, most commonly as calcite. As a result, it is important to understand the impact that calcite addition has on the interpretation of the ω and ψ coefficients. To investigate this effect we performed a synthetic experiment by increasing the amount of CaO in a sediment composition, and recalculated the ω and ψ coefficients. The results of this experiment are shown in Figure S-2. Addition of calcite introduces a spurious reduction in weathering intensity. A spuriously more felsic protolith is also introduced, although the magnitude of this effect is much more minor. It is important to minimise the effect of these biases by screening samples from our dataset which are clearly affected by carbonate addition. Lacking mineralogical data it is generally challenging to identify carbonate contaminated samples. One approach is simply to remove samples which have CaO values above a certain cut-off value. However, given that cation exchange is another process which can increase the CaO this approach may be removing sediments which do not contain significant carbonate but simply have absorbed Ca. As a result, we identify the maximum amount of calcium which could be expected to be found in a sediment, if all of the sodium exchanges for calcium, for a standard range of protoliths. This corresponds to a sediment which derives from a basalt but has not undergone significant weathering. Hence, any sediment which has more calcium than this cut off value, if all the sodium is also exchanged, must also contain calcite and is thus excluded from consideration. This procedure is detailed more explicitly in the accompanying code (github.com/AlexLipp/crustal-comp).

Despite this filter, it is still likely that small amounts of calcite are present in many sediments from our dataset. As a result, our interpreted weathering intensities are likely an underestimate. To make sure that this bias is not the cause of the temporal trends in weathering intensity we see, we repeated our analysis with a more stringent carbonate filter (excluding all samples which had a positive CaO residual when cation exchange is not considered), but we observed similar trends. This suggests that whilst our data does likely incorporate the effect of carbonate addition, it does not affect the conclusions we have drawn.

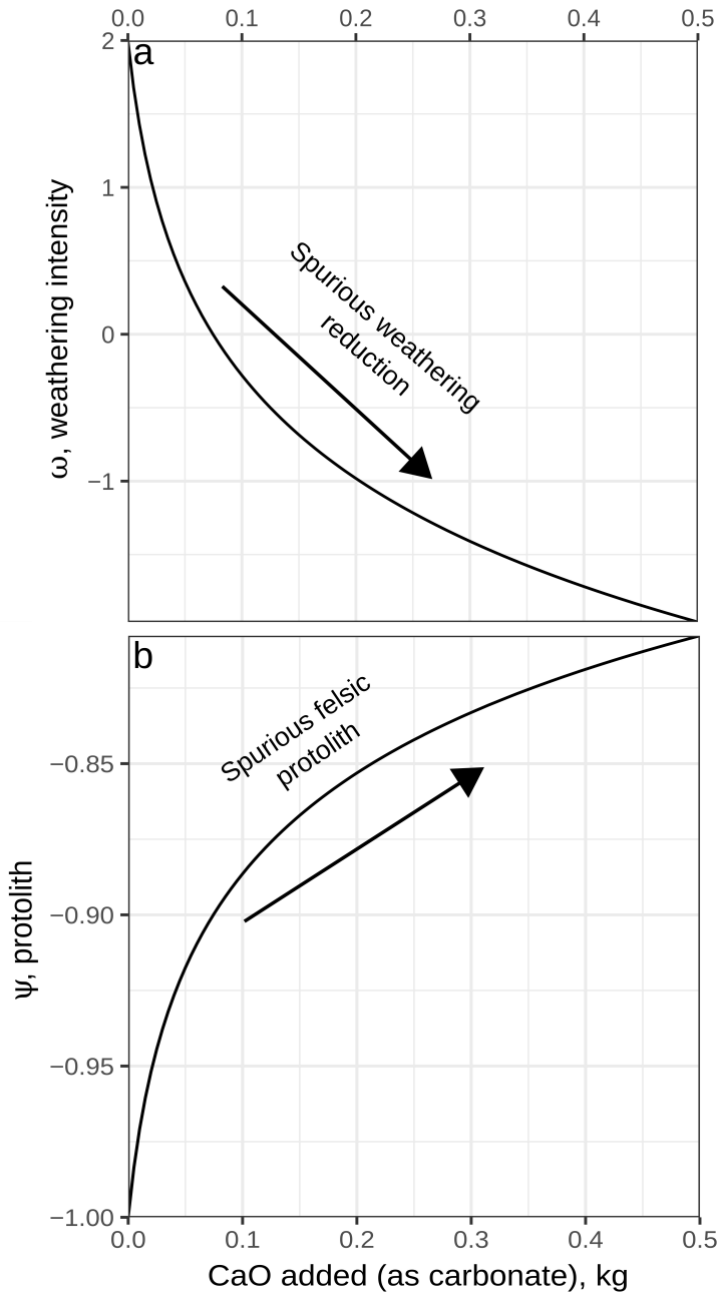

Figure S-2 Exploring biases due to calcite addition. **(a)** Changes in ω coefficient resulting when increasing amounts of calcite are added to a composition with inital (ω, ψ) values of (2, -1). This suggests that the presence of any carbonate results in a spurious reduction in weathering intensity. **(b)** Changes in ψ coefficient resulting from same synthetic experiment as panel (a). Calcite addition therefore introduces a spurious felsic bias. Note however that this bias is much smaller in magnitude than the bias introduced for ω.

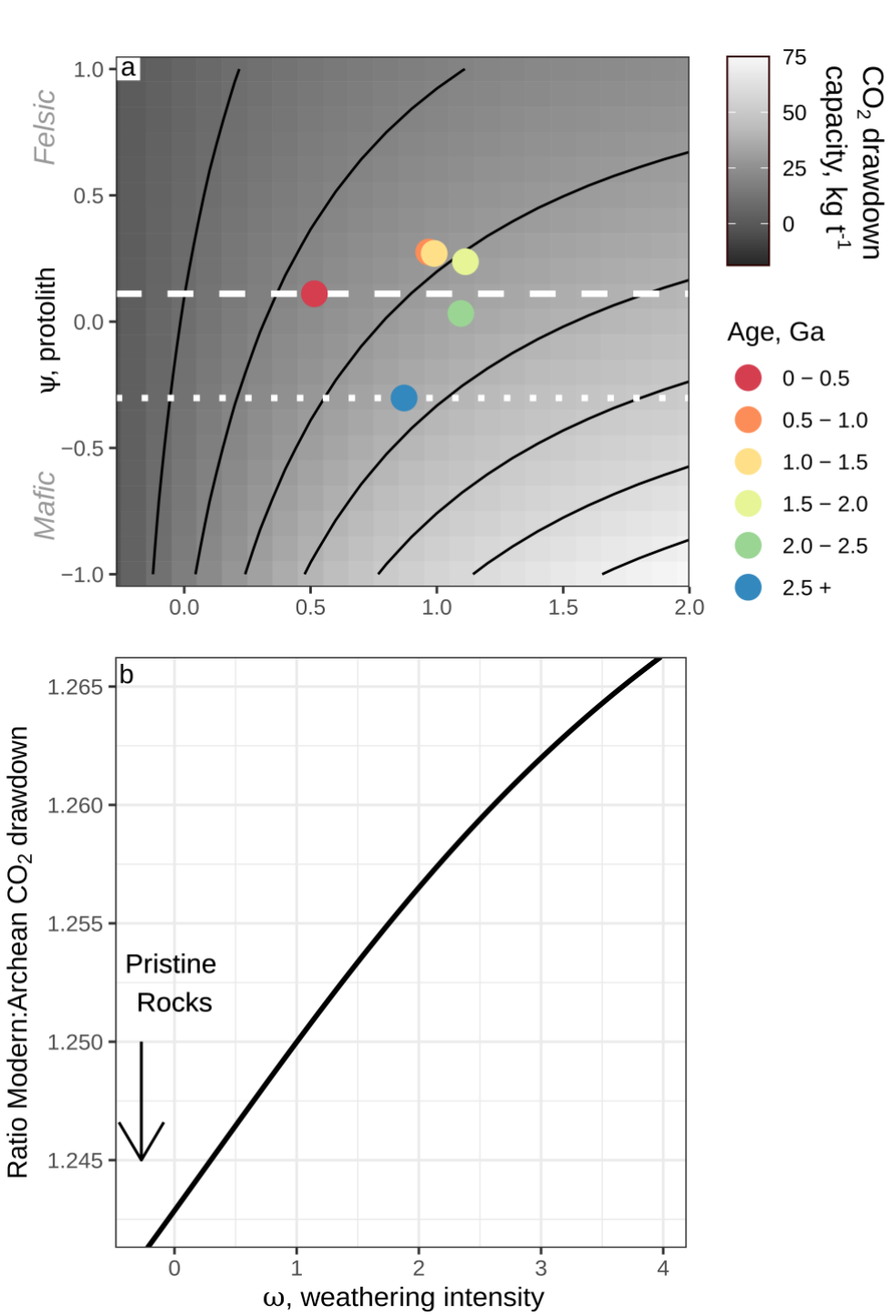

Figure S-3 CO_2 drawdown capacity of sediments through time. **(a)** ω–ψ plot overlain with contours of CO_2 drawdown capacity, calculated using the methods detailed in the main text. This is the amount of CO_2 that could be transferred from the atmosphere to the lithosphere via weathering, assuming all acidity is donated by carbonic acid. Value is given as kg of CO_2 removed from atmosphere per tonne rock eroded. Sediments with more mafic protoliths and greater weathering intensities result in higher potential CO_2 drawdown. Coloured points are the composite sediments from the indicated time periods. Dashed line corresponds to ψ value of period 0–0.5 Ga; Dotted line period 2.5 + Ga. **(b)** Ratio of Archean to present (0–0.5 Ga) CO_2 drawdown capacities for different ω values. Line is generated by dividing the

CO_2 drawdown capacity along the dotted line by the values along the dashed line in panel (a). For the same weathering intensity, the Archean sedimentary protolith sequestered ~25 % more CO_2.

Sampling Bias

The samples in our dataset are not homogenously distributed in time (Fig. S-1). As a result, for periods of low sample density, the average weathering trend we calculate will be more uncertain. To quantify this changing uncertainty interval we utilised a bootstrap resampling technique. Here, we resampled our dataset 1000 times with replacement. For each of these resampled datasets we generated a smoothed trend with the same 30 Myr Gaussian kernel. Then for each point in time we simply calculate the minimum and maximum possible values of the smoothed trend from these 1000 possible trends. These envelopes are shown as grey lines in Figure 3. This bounding envelope is wider in periods of lower sampling density reflecting the greater uncertainty of the average trend (Fig. S-1a).

An additional issue that can arise is if some particular stratigraphic units are 'oversampled' due to various reasons including accessibility of samples and particular economic interest. To investigate the robustness of our findings in the Phanerozoic against this issue we generate an analogous figure to Figure 3 but we instead take the mean ω value for individual stratigraphic units. We subsequently smooth these unit-averaged data points in the same way as before (*i.e.* applying a Gaussian filter of 30 Myr bandwidth and calculating the bootstrap uncertainties). The results of this analysis are displayed in Figure S-4. The location of the peaks and troughs in this trend are largely similar to the original trend in Figure 3. The trough in weathering intensity during the Ordovician/Silurian in Figure 3 is not however visible in this unit-averaged trend. It is notable that due to the smaller number of data points the bootstrap uncertainties are much higher than if samples are treated individually. This is particularly true for regions where only a small number of stratigraphic units have been sampled (Fig. S-1b).

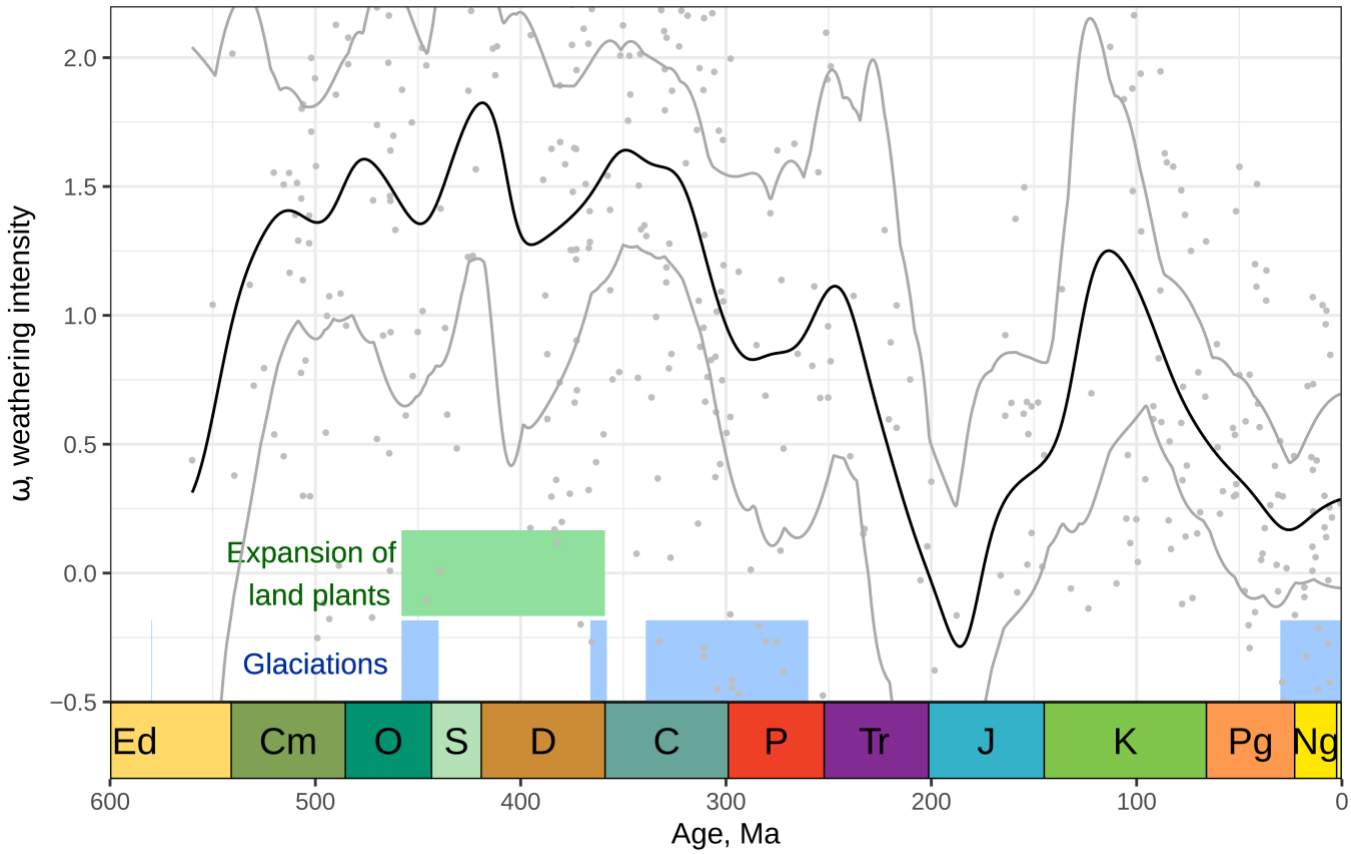

Figure S-4 Weathering trend after averaging of ω values within stratigraphic units. Grey points indicate average ω value of individual stratigraphic units. Black curve generated by smoothing data using 30 Myr Gaussian kernel. Grey lines indicate bounding envelope of 1000 bootstrap resamples of data. The general shape of this trend is similar to that displayed in Figure 3 although without a reduction in weathering intensity during the Ordovician/Silurian. Note the much greater uncertainty envelope than if all samples are treated individually.

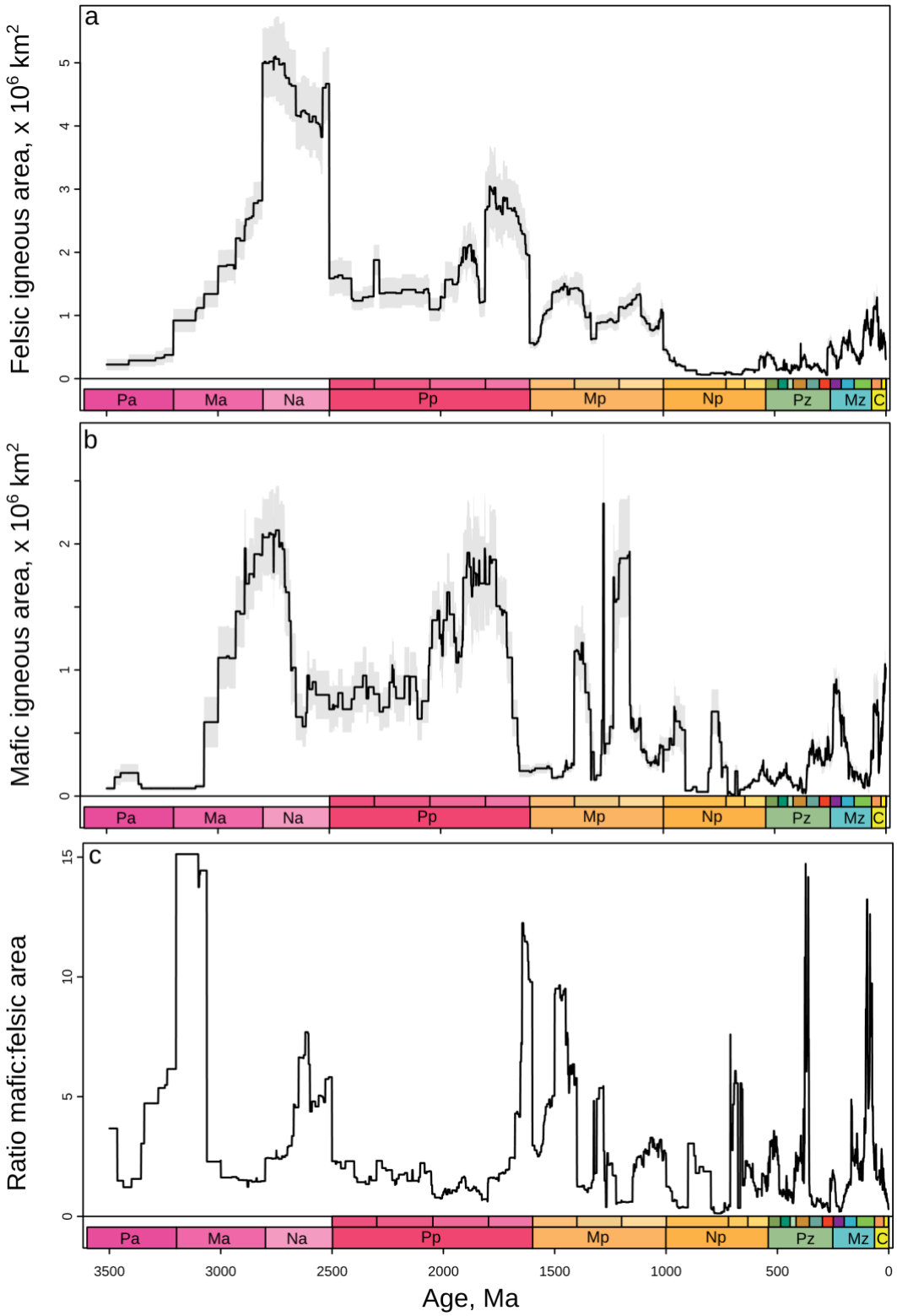

Figure S-5 Areal extent of igneous rocks through time in Macrostrat database of geologic columns in North America (Peters *et al.*, 2018). **(a)** Felsic area. **(b)** Mafic area. **(c)** Ratio of felsic to mafic area. Any secular trend in the mafic:felsic ratio is lower in magnitude than the short-term variability. This observation is consistent with the largely constant protolith diversity shown in Figure 2. Igneous rocks in the database are divided into 'felsic' and 'mafic' lithologies; all lithology classes can be found at macrostrat.org/api/defs/lithologies?all. Note that mafic and felsic rocks can co-occur in the same stratigraphic unit and are counted in both instances. Not all igneous rocks fall into one of these general

lithology groups, and some names widely used in field descriptions (on which the Macrostrat classification is based, *e.g.*, 'granite') are based on very broad compositional information. The Macrostrat API calls to extract data for this figure are found in the code repository.

Supplementary Information References

Aitchison, J. (1986) *The statistical analysis of compositional data*. Chapman and Hall, London, UK.

Bjørlykke, K., Jahren, J. (2012) Open or closed geochemical systems during diagenesis in sedimentary basins: Constraints on mass transfer during diagenesis and the prediction of porosity in sandstone and carbonate reservoirs. *AAPG Bulletin* 96, 2193–2214.

Brimhall, G.H., Dietrich, W.E. (1987) Constitutive mass balance relations between chemical composition, volume, density, porosity, and strain in metasomatic hydrochemical systems: Results on weathering and pedogenesis. *Geochimica et Cosmochimica Acta* 51, 567–587.

Cerling, T.E., Pederson, B.L., Damm, K.L.V. (1989) Sodium-calcium ion exchange in the weathering of shales: Implications for global weathering budgets. *Geology* 17, 552–554.

Devaraju, T.C., Sudhakara, T.L., Kaukonen, R.J., Viljoen, R.P., Alapieti, T.T., Ahmed, S.A., Sivakumar, S. (2010) Petrology and geochemistry of greywackes from GoaDharwar sector, western Dharwar Craton: Implications for volcanoclastic origin. *Journal of the Geological Society of India* 75, 465–487.

Fedo, C.M., Eriksson, K.A., Krogstad, E.J. (1996) Geochemistry of shales from the Archean (~3.0 Ga) Buhwa Greenstone Belt, Zimbabwe: Implications for provenance and source-area weathering. *Geochimica et Cosmochimica Acta* 60, 1751–1763.

Jaffrés, J.B.D., Shields, G.A., Wallmann, K. (2007) The oxygen isotope evolution of seawater: A critical review of a long-standing controversy and an improved geological water cycle model for the past 3.4 billion years. *Earth-Science Reviews* 83, 83–122.

Jiang, H., Lee, C.-T.A. (2019) On the role of chemical weathering of continental arcs in long-term climate regulation: A case study of the Peninsular Ranges batholith, California (USA). *Earth and Planetary Science Letters* 525, 115733.

Lipp, A.G., Shorttle, O., Syvret, F., Roberts, G.G. (2020) Major Element Composition of Sediments in Terms of Weathering and Provenance: Implications for Crustal Recycling. *Geochemistry, Geophysics, Geosystems* 21, e2019GC008758.

Lupker, M., France-Lanord, C., Lartiges, B. (2016) Impact of sediment–seawater cation exchange on Himalayan chemical weathering fluxes. *Earth Surface Dynamics* 4, 675–684.

Macdonald, F.A., Swanson-Hysell, N.L., Park, Y., Lisiecki, L., Jagoutz, O. (2019) Arc-continent collisions in the tropics set Earth's climate state. *Science* 364, 181–184.

McMahon, W.J., Davies, N.S. (2018) Evolution of alluvial mudrock forced by early land plants. *Science* 359, 1022–1024.

Nesbitt, H.W., Young, G.M., Bosman, S.A. (2009) Major and trace element geochemistry and genesis of supracrustal rocks of the North Spirit Lake Greenstone belt, NW Ontario, Canada. *Precambrian Research* 174, 16–34.

Peters, S.E., Husson, J.M., Czaplewski. J. (2018) Macrostrat: A Platform for Geological Data Integration and Deep-Time Earth Crust Research. *Geochemistry, Geophysics, Geosystems* 19, 1393–1409.

Pu, J.P., Bowring, S.A., Ramezani, J., Myrow, P., Raub, T.D., Landing, E., Mills, A., Hodgin, E., Macdonald, F.A. (2016) Dodging snowballs: Geochronology of the Gaskiers glaciation and the first appearance of the Ediacaran biota. *Geology* 44, 955–958.

R Core Team (2018) *R: A Language and Environment for Statistical Computing*. Vienna, Austria.

Sayles, F.L., Mangelsdorf, P.C. (1979) Cation-exchange characteristics of Amazon River suspended sediment and its reaction with seawater. *Geochimica et Cosmochimica Acta* 43, 767–779.

Sepkoski, J.J. (1993) Ten Years in the Library: New Data Confirm Paleontological Patterns. *Paleobiology* 19, 43–51.

Sun, X., Higgins, J., Turchyn, A.V. (2016) Diffusive cation fluxes in deep-sea sediments and insight into the global geochemical cycles of calcium, magnesium, sodium and potassium. *Marine Geology* 373, 64–77.

Torres, M.A., West, A.J., Li, G. (2014) Sulphide oxidation and carbonate dissolution as a source of CO_2 over geological timescales. *Nature* 507, 346–349.

Van Rossum, G., Drake, F.L. (2009) *Python 3 Reference Manual*. Scotts Valley, CA.

Wallmann, K., Aloisi. G., Haeckel, M., Tishchenko, P., Pavlova, G., Greinert, J., Kutterolf, S., Eisenhauer, A. (2008) Silicate weathering in anoxic marine sediments. *Geochimica et Cosmochimica Acta* 72, 2895–2918.

White, A.F., Bullen, T.D., Schulz, M.S., Blum, A.E., Huntington, T.G., Peters, N.E. (2001) Differential rates of feldspar weathering in granitic regoliths. *Geochimica et Cosmochimica Acta* 65, 847–869.

Young, K.E., Evans, C.A., Hodges, K.V., Bleacher, J.E., Graff, T.G. (2016) A review of the handheld X-ray fluorescence spectrometer as a tool for field geologic investigations on Earth and in planetary surface exploration. *Applied Geochemistry* 72, 77–87.